APPLICATION OF THE MIMO RADAR TECHNIQUE FOR LESION CLASSIFICATION IN UWB BREAST CANCER DETECTION

Yifan Chen[1], *Ian James Craddock*[2], *Panagiotis Kosmas*[3], *Mohammad Ghavami*[3], *and Predrag Rapajic*[1]

[1]School of Engineering, University of Greenwich, United Kingdom, (E-mail: Y.Chen@gre.ac.uk)
[2]Department of Electrical and Electronic Engineering, University of Bristol, United Kingdom
[3]Division of Engineering, King's College London, United Kingdom

ABSTRACT

In ultra-wideband (UWB) breast imaging, it has been shown that benign and malignant masses, which usually possess remarkable architectural differences, could be distinguished by exploiting their morphology-dependent microwave backscatter. The complex natural resonances (CNRs) of the backscatter signature can be derived from the late-time target response, where the damping factors vary with the border profiles of lesions. As an extension to our previous work (Chen et al. 2008), here we investigate the potential advantage of multiple-input multiple-output (MIMO) radars to enhance the resonance scattering phenomenon in tissue differentiation. Based on the observed damping factors and the receiver operating characteristics (ROC) at different classifiers, which correspond to various diversity paths in the MIMO radar system, the selection combining fusion scheme is proposed for robust lesion classification. We also provide numerical examples to demonstrate the efficacy of the proposed imaging technique.

1. INTRODUCTION

In recent years, the use of ultra-wideband (UWB) radar techniques for breast cancer detection has attracted much research interest [1-3]. For UWB breast imaging, recent breast tissue dielectric-spectroscopy measurements have suggested that the malignant-to-benign dielectric contrast may not be sufficiently high to allow for tissue classification based on backscatter intensity [4]. Alternatively, it is well known that the architectural distortion in breast parenchyma can aid in distinguishing malignant tumors from benign masses [5]. For example, mammographic image analysis shows that cancerous tissues usually have an irregular appearance, and are surrounded by a radiating pattern of linear spicules. Conversely, benign masses are usually well-circumscribed and roughly elliptical [5]. Accordingly, the microwave signature could be potentially useful for discrimination between benign and malignant lesions [2, 3].

This paper investigates the problem of malignant/benign tissue discrimination assuming that the presence and location of a strong scattering center ("Target") has been successfully identified through a breast cancer detection algorithm (see e.g., [1]). The complex natural resonances (CNRs) of the target late-time response are extracted and their interrelationship with the morphological features of lesions is analyzed [3]. We will focus on a multiple-input multiple-output (MIMO) radar architecture, which can transmit multiple probing signals that may be chosen arbitrarily and independently. This waveform diversity enables superior performance of phenomenon-of-interest detection [6]. For the current setup of UWB breast cancer detection as illustrated in Fig. 1, the incident waveform transmitted from each array element is chosen from the family of modulated and modified Hermite polynomials (MMHPs). The relevant phenomenon-of-interest observed at Antenna A_{k_2} induced by the probing signal from Antenna A_{k_1} is considered to be the damping factor of a specific CNR, X_{k_1,k_2}. As shown in [3], X_{k_1,k_2} is a random variable due to the nondeterministic nature of the lesion shape. Furthermore, the statistical properties of X_{k_1,k_2} vary with the border profiles of lesions, which in turn are correlated with the pathologic features of the tissue [5]. These phenomena set up a strong basis for the tissue differentiation technique proposed in the current work.

The remainder of the paper is organized as follows. In Section 2, we briefly discuss the method to generate two-dimensional (2D) breast masses with various levels of shape irregularities [3]. In Section 3, we derive the empirical distribution functions of X_{k_1,k_2} through comprehensive simulations. In Section 4, the selection combining fusion is proposed for robust lesion classification. Numerical examples are then provided in Section 5 to demonstrate the effectiveness of the proposed technique. Finally, some concluding remarks are drawn in Section 6.

2. RANDOM TARGET MODELS

When the patient lies in a supine position, the 2D axial view of the breast could be approximated by a semi-circle [1] as shown in Fig. 1. The breast and antennas are immersed in a coupling medium with electrical properties similar to those of healthy breast tissues [3]. Subsequently, a first-order Debye dispersion equation will be employed to describe the frequency dependence of the dielectric properties of nominal healthy tissues [1]. At any frequency, the actual dielectric properties for normal and deceased breast tissues range over a specified percentage variation μ about the nominal value.

Tumors normally have more irregular or asymmetrical geometries than benign anomalies and show more deviation from a perfect ellipse [2, 3, 5]. Different approaches to modelling these anomalies have appeared in the literature (see e.g.,[2, 3]). In [3, 5], the lesion boundaries are approximated by polygons. The similar approach is applied in this paper to simulate malignant and benign lesions. First, we establish a

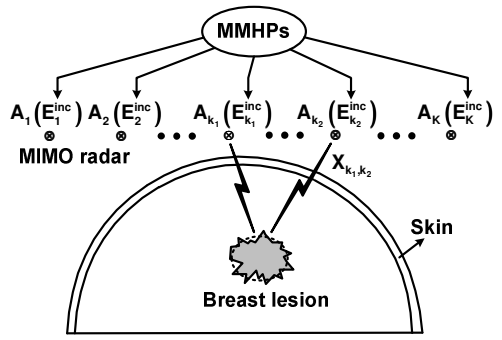

Figure 1: An UWB MIMO radar system for breast tissue differentiation

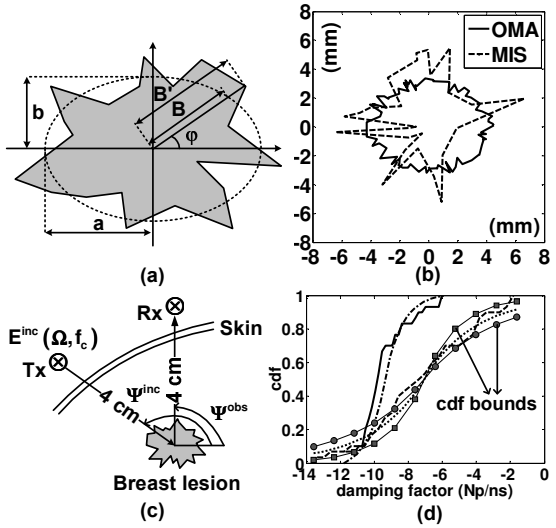

Figure 2: (a) Generation of a lesion border from a baseline ellipse, (b) examples of OMA and MIS targets, (c) system setup for characterizing the statistical properties of damping factors, and (d) cdfs of OMA and MIS data for $\Omega = 1$, $\Psi^{obs} = 150°$, and $f_c = 1$ GHz: – empirical (OMA), – · – Laplace (OMA), – – empirical (MIS), ⋯ Laplace (MIS)

baseline ellipse defined in the polar coordinate as $B(\varphi) = ab/\sqrt{a^2 \sin^2 \varphi + b^2 \cos^2 \varphi}$, where a and b are the semi-major and semi-minor axes, and φ is the angle as indicated in Fig. 2(a). The next step is to modify the initial shape to produce the proper mass border with various irregularities. The simulation routine consists of the following stages:

(i) Define the number of sides of the polygonal approximation to the mass boundary, Q;

(ii) Generate $\varphi_q \sim \mathcal{U}(0, 2\pi]$, ($q = 1, 2, \cdots, Q$), where $\mathcal{U}$ denotes a uniform distribution;

(iii) For each φ_q, define the distribution of the border deviation profile $\zeta(\varphi_q) \sim \mathcal{U}(-\Delta B, +\Delta B]$, and apply it to the elliptical profile in a multiplicative fashion as (see also Fig. 2(a)) $B'(\varphi_q) = B(\varphi_q)(1+\zeta(\varphi_q))$.

These two parameters, Q and ΔB, determine the ruggedness of the mass boundary.

To simplify our analysis, we consider a *binary* classification of the lesion morphology. The shape of each random target is assumed to fall into one of the following two categories: oval/macrolobulated (OMA) or microlobulated/spiculated (MIS). The OMA class includes targets that correspond to round, oval, or macrolobulated shape descriptors, which leads to the acceptance of Hypothesis H_0 ("Target is benign"). On the contrary, the MIS class exhibits fine-scale undulations over the target surface or spicules radiating from the body of the target, which leads to the acceptance of Hypothesis H_1 ("Target is malignant"). As observed in [3], the circumference texture becomes considerably rugged as Q decreases and ΔB increases. Therefore, we obtain the OMA targets by generating the two random variables Q and ΔB, where $Q \sim \mathcal{U}$ [80, 100] and $\Delta B \sim \mathcal{U}$ [0.1, 0.3]. On the other hand, the MIS lesions are simulated with $Q \sim \mathcal{U}$ [10, 30] and $\Delta B \sim \mathcal{U}$ [0.8, 1]. These ranges of Q and ΔB are chosen to reflect the distinctive features of these two types of anomalies. Fig. 2(b) plots the mass border deviations corresponding to the OMA and MIS targets.

The UWB MIMO radar consists of a multistatic antenna array, where K antennas $A_1, \cdots, A_K$ are probing the breast as shown in Fig. 1. As the commonly-used UWB signals fit extremely well into the Hermite polynomials, the incident pulse transmitted from the kth ($1 \le k \le K$) antenna is selected from the family of MMHP waveforms proposed in [7]

$$E_k^{inc} = \exp\left(-\frac{t^2}{4T_p^2}\right) h_{\Omega_k}\left(\frac{t}{T_p}\right) \cos\left(2\pi f_{c,k} t\right) \qquad (1)$$

where $\Omega_k = 0, 1, 2, \cdots$, h_{Ω_k} is the Ω_kth-order Hermite polynomial, T_p controls the duration of the pulses, and $f_{c,k}$ is the carrier frequency. To test our algorithm with simulated data, we follow the same approaches in [3] to derive the backscatter signature at any observation point and extract the CNRs from the late-time component of the scattered waveform.

3. STATISTICAL PROPERTIES OF OBSERVED DAMPING FACTORS

The system setup used to generate synthetic data for our quantitative analysis is shown in Fig. 2(c). The transmit (Tx) and receive (Rx) antennas are positioned in a circle with radius of 4 cm around the lesion. For data acquisition, the Tx antenna transmits an MMHP pulse $E^{inc}(\Omega, f_c)$ where Ω and f_c are the pulse order and modulation frequency, respectively, and T_p is fixed as 50 ps (cf. (1)). The following Debye parameters are used to fit experimental results for nominal breast tissues ($\varepsilon_s = 10$, $\varepsilon_\infty = 7$, $\sigma_s = 0.15$ S/m, $\tau = 7.0$ ps) (see [1] for the definitions of various Debye parameters). A 0.2-cm skin layer with the relative dielectric constant $\varepsilon_r = 36.0$ and conductivity $\sigma = 4.0$ S/m is also included [1]. Furthermore, the slab model is applied to derive the transmission coefficient through the skin [3]. The dielectric properties of the target are obtained by setting $\mu = 4$ (see also Section 2).

We build a library of random dielectric masses with shapes that fall into either OMA or MIS category. The semi-major and semi-minor axes of the baseline ellipse are assumed to be 4 mm and 3 mm, respectively. We generate 30 independent target realizations for each shape class. To examine the isolated effect of different design parameters of the MIMO radar, two different scenarios are considered:

(i) The Tx and Rx antennas are at the same location with $\Psi^{inc} = \Psi^{obs} = 150°$. $\Omega = 1$ and $f_c = 0, 1, 2, 3, 4$ GHz;

(ii) The Tx antenna location is fixed with $\Psi^{inc} = 150^o$ while the Rx antenna location varies with angle so that $\Psi^{obs} = 30^o, 60^o, 90^o, 120^o, 150^o$. For this case, $\Omega = 1$ and $f_c = 1$ GHz.

The CNRs of the backscatter waveforms are then extracted. In general, two most dominant resonances can be obtained from the backscatter [3]. We found through extensive simulations that out of these two frequencies, the high-frequency resonance provides better classification performance as compared to the low-frequency one by offering more sensitive lesion discrimination through statistical inference of the damping factors. Therefore, we will focus on the high-frequency CNR in the current work.

The empirical cumulative distribution functions (cdfs) of the damping factors are illustrated in Fig. 2(d) for $\Omega = 1$, $\Psi^{obs} = 150^o$, and $f_c = 1$ GHz. The following important observations can be made. Firstly, the damping factors for OMA lesions fall within a narrow range, where the empirical cdf agrees well with a truncated Laplace distribution as shown in Fig. 2(d). The theoretical pdf can be expressed as

$$p_0(X) = \frac{\mathcal{K}_0}{2W_0}\exp\left(-\frac{\left|X-\bar{X}_0\right|}{W_0}\right),\ X_{\min} \le X \le X_{\max} \quad (2)$$

where X denotes a random damping factor, and $\bar{X}_0$ and W_0 are the location and scale parameters, respectively. In (2), $X_{\min}$ and $X_{\max}$ are the lower and upper bounds of X for OMA targets. $\mathcal{K}_0$ is a normalization factor to ensure that $p_0(X)$ is a pdf. Secondly, contrary to the OMA class, the damping factors for MIS lesions are scattered over a much wider range due to more ill-defined target geometries. The empirical data could be fit with a general Laplace pdf

$$p_1(X) = \frac{1}{2W_1}\exp\left(-\frac{\left|X-\bar{X}_1\right|}{W_1}\right) \quad (3)$$

where $\bar{X}_1$ and W_1 are model parameters. Thirdly, it is more difficult to characterize p_1 exactly due to the limited simulated data and the widely-spread damping factors. Hence, it is supposed that p_0 is completely specified while p_1 belongs to an uncertainty class $\mathcal{P}_1$, which is defined by assuming that W_1 is a random variable with an uniform pdf, $W_1 \sim \mathcal{U}[W_{1,\min}, W_{1,\max}]$. Fig. 2(d) plots the best-fit Laplace cdf for the MIS data and the corresponding cdf bounds, which are obtained by setting $W_{1,\min} = 2$ and $W_{1,\max} = 4$. $\bar{X}_1$ remains unchanged. In general, $W_0 = 1$ and $1 \le W_1 \le 4$ for all the simulation scenarios. Finally, the cdf curves for OMA and MIS data are well separated in the cdf space, which demonstrates the feasibility of lesion discrimination through statistical inference of the damping factors.

4. DATA FUSION RULE FOR ROBUST LESION CLASSIFICATION

4.1 Basic Concepts

In a MIMO-radar-based breast lesion classification system, a total number of K^2 classifiers C_{k_1,k_2} ($1 \le k_1,k_2 \le K$) observe data generated according to either H_0 ("Target is benign") or H_1 ("Target is malignant"). The classifier C_{k_1,k_2} corresponds to the spatial diversity path from Antenna A_{k_1} to Antenna A_{k_2}, and the observable is the random damping factor X_{k_1,k_2}. Subsequently, a decision $U_i^{(C_{k_1,k_2})}$ (-1 if H_0 is accepted and 1 otherwise) about the true hypothesis is to be made based on X_{k_1,k_2} subject to its distribution under H_0 (given as $p_0^{(C_{k_1,k_2})}$) and H_1 (given as $p_1^{(C_{k_1,k_2})}$), where $p_1^{(C_{k_1,k_2})}$ belongs to the uncertainty class $\mathcal{P}_1^{(C_{k_1,k_2})}$. Mathematically, $U_i^{(C_{k_1,k_2})} = \gamma_i^{(C_{k_1,k_2})}\left(X_{k_1,k_2}\right) \in \{-1,1\}$, where $\gamma_i^{(C_{k_1,k_2})}$ is the ith local admissible strategy. The local decisions $U_i^{(C_{k_1,k_2})}$, together with $\gamma_i^{(C_{k_1,k_2})}$ and their corresponding probability of detection $P_{D,i}^{(C_{k_1,k_2})}$ and probability of false alarm $P_{F,i}^{(C_{k_1,k_2})}$ are sent to a data fusion center for a global decision $U \in \{-1,1\}$. Our goal is to design an optimal fusion rule that maximizes the asymptotic error exponent $\mathcal{E}$, which is given by the Chernoff information under the Bayesian framework [8]. For the ease of analysis, we consider a special case of Chernoff information, the Bhattacharyya distance [8]. The following concepts are introduced to facilitate the analysis of the fusion structure. For simplicity, the superscript (C_{k_1,k_2}) and the subscripts i and k_1,k_2 are omitted.

Definition 1 (Uncertainty Class): An uncertainty class $\mathcal{P}_1$ is a set of neighbourhood distributions containing $p_1(x;\Theta_1)$ under Hypothesis H_1. The dummy variable x represents the observed data X, and Θ_1 is the model parameter for the uncertainty class, which is a random variable following the distribution function $f_{\Theta_1}(\Theta_1)$.

Definition 2 (Receiver Error Exponent Characteristics (REEC)): A REEC curve represents a curve joining a set of points with the coordinates (P_F, $\mathcal{E}$). Each point denotes an admissible strategy γ, which produces false positives with a probability P_F and the achievable error exponent $\mathcal{E}$ given by the Bhattacharyya distance.

Remark 1: The optimum test for two hypotheses is the log-likelihood-ratio (LLR) test, which usually involves comparison of the observed data X to a threshold X_{th} [8]. Without loss of generality, it is assumed that H_1 is accepted if $X \ge X_{th}$ and H_0 is accepted otherwise. In other words, a local decision U can be calculated as $U = \gamma(X) = \mathrm{sgn}(X - X_{th})$ where sgn is the signum function. Subsequently, the false positive rate P_F is related to X_{th} through the following equation $P_F = \int_{X_{th}}^{X_{\max}^{(H_0)}} p_0(x)\,dx$, where $X_{\max}^{(H_0)}$ is the maximum observed data conditional on H_0. Apparently, X_{th} can be expressed as a function of P_F, $X_{th} = \mathcal{F}(P_F)$. The next step is to derive the probability of detection as $P_D = \int_{X_{th}}^{X_{\max}^{(H_1)}} p_1(x;\Theta_1)\,dx = \int_{\mathcal{F}(P_F)}^{X_{\max}^{(H_1)}} p_1(x;\Theta_1)\,dx$, where $X_{\max}^{(H_1)}$ is

the maximum observed data conditional on H_1. Finally, the Bhattacharyya distance can be derived as [8]

$$\begin{aligned}\mathcal{E} &= -\log_2\left\{(1-P_{\mathrm{F}})^{\frac{1}{2}}(1-P_{\mathrm{D}})^{\frac{1}{2}}+P_{\mathrm{F}}^{\frac{1}{2}}P_{\mathrm{D}}^{\frac{1}{2}}\right\} \\ &= -\log_2\left\{(1-P_{\mathrm{F}})^{\frac{1}{2}}\left[1-\int_{\mathcal{F}(P_{\mathrm{F}})}^{X_{\max}^{(H_1)}}p_1(x;\Theta_1)dx\right]^{\frac{1}{2}}+P_{\mathrm{F}}^{\frac{1}{2}}\left[\int_{\mathcal{F}(P_{\mathrm{F}})}^{X_{\max}^{(H_1)}}p_1(x;\Theta_1)dx\right]^{\frac{1}{2}}\right\}\end{aligned} \tag{4}$$

Following (4), $\mathcal{E}$ is a random variable at each P_{F} with distribution dependent on $f_{\Theta_1}(\Theta_1)$.

To provide a statistical characterization of reliable lesion classification, the notion of *outage* is introduced.

Definition 3 (Outage Probability): Consider a classifier with unspecified conditional probability distributions of the observations. At each false positive rate P_{F}, the outage probability P_{out} is defined as the probability for which the classifier is in a state of outage (i.e., failure) for hypothesis testing at a certain error exponent $\mathcal{E}_{\mathrm{out}}$. Mathematically, P_{out} = $\Pr(\mathcal{E} \le \mathcal{E}_{\mathrm{out}})$ where $\Pr(\cdot)$ denotes probability.

On the basis of Definition 3, we further define the outage error exponent as follows.

Definition 4 (Outage Error Exponent): Consider a classifier with unspecified conditional probability distributions of the observations. At each false positive rate P_{F}, the outage error exponent is defined as the maximum error exponent that can be achieved across all possible realizations of conditional probability distributions of the observations, $p_1 \in \mathcal{P}_1$, for a prescribed outage probability P_{out}.

Remark 2: One conventional way to design decision rules when the conditional pdfs of the observations are not specified completely is the *minimax* approach [9], where the goal is to optimize the worst case performance over the uncertainty class. However, this operational point will be of little practical significance if it is of low likelihood. A more statistically-relevant solution is to optimize the classifier performance along the receiver outage error exponent characteristics (ROEEC) curve, where the error exponent is defined for a sufficiently low outage probability.

4.2 Selection Combining Fusion

The selection combining fusion rule is proposed to choose one classifier that yields the best outage error exponent across all classifiers and across all admissible strategies, i.e.,

$$\max_{k_1,k_2,P_{\mathrm{F}}} \mathcal{E}_{\mathrm{out}}^{(C_{k_1,k_2})}(P_{\mathrm{F}}) \text{ s.t. } \Pr\left(\mathcal{E}^{(C_{k_1,k_2})}(P_{\mathrm{F}}) \le \mathcal{E}_{\mathrm{out}}^{(C_{k_1,k_2})}(P_{\mathrm{F}})\right) = P_{\mathrm{out}} \tag{5}$$

Where $\mathcal{E}_{\mathrm{out}}^{(C_{k_1,k_2})}(P_{\mathrm{F}})$ represents the outage error exponent at a false positive rate P_{F} for Classifier C_{k_1,k_2}. The above optimization process can be realized through the following steps:

(i) Plot the ROEEC linking a series of points (P_{F}, $\mathcal{E}_{\mathrm{out}}^{(C_{k_1,k_2})}$) for each classifier C_{k_1,k_2}, conditional on P_{out};

(ii) Convert the ROEEC into the receiver operating characteristics (ROC) curve, where $\mathcal{E}_{\mathrm{out}}^{(C_{k_1,k_2})}$ is changed to the corresponding probability of detection $P_{\mathrm{D,out}}^{(C_{k_1,k_2})}$;

(iii) Produce the maximum realizable ROC (MRROC) predicted by the convex hull containing all the ROC curves associated with all classifiers [10]. The vertex points of the convex hull will be points corresponding to the existing classifiers generated by Step (ii). The facets of the hull are line segments with an existing classifier at each end point;

(iv) Identify the optimal operational point on the MRROC with the best asymptotic error exponent.

The general algorithms discussed above can be readily applied to the lesion classification problem, where the pdfs of damping factors for OMA and MIS targets follow the Laplace distributions in (2) and (3). Moreover, p_0 is completely specified while p_1 belongs to an uncertainty class $\mathcal{P}_1$, which is defined by assuming that $W_1 \sim \mathcal{U}[W_{1,\min}, W_{1,\max}]$. Subsequently, the following results can be established.

Proposition 1: If the distributions of random damping factors satisfy the empirical models presented in Section 3, the true positive rate corresponding to the outage error exponent $\mathcal{E}_{\mathrm{out}}$ for an outage probability P_{out} is given by

Case I: $\bar{X}_1 < \bar{X}_0$

$$P_{\mathrm{D,out}} = \begin{cases} \frac{1}{2}\exp\left\{\dfrac{\bar{X}_0-\bar{X}_1+W_0\ln\left\{2P_{\mathrm{F}}/\mathcal{K}_0+\exp\left[\left(X_{\min}-\bar{X}_0\right)/W_0\right]\right\}}{W_{1,\min}+\left(W_{1,\max}-W_{1,\min}\right)P_{\mathrm{out}}}\right\}, & \text{if } X_{\min} \le X_{\mathrm{th}} < \bar{X}_1 \\ 1-\frac{1}{2}\exp\left\{-\dfrac{\bar{X}_0-\bar{X}_1+W_0\ln\left\{2P_{\mathrm{F}}/\mathcal{K}_0+\exp\left[\left(X_{\min}-\bar{X}_0\right)/W_0\right]\right\}}{W_{1,\max}-\left(W_{1,\max}-W_{1,\min}\right)P_{\mathrm{out}}}\right\} & \text{if } \bar{X}_1 \le X_{\mathrm{th}} < \bar{X}_0 \\ 1-\frac{1}{2}\exp\left\{-\dfrac{\bar{X}_0-\bar{X}_1-W_0\ln\left\{\left(2\mathcal{K}_0-2P_{\mathrm{F}}\right)/\mathcal{K}_0-\exp\left[\left(X_{\min}-\bar{X}_0\right)/W_0\right]\right\}}{W_{1,\max}-\left(W_{1,\max}-W_{1,\min}\right)P_{\mathrm{out}}}\right\} & \text{if } \bar{X}_0 \le X_{\mathrm{th}} \le X_{\max} \end{cases} \tag{6}$$

Case II: $\bar{X}_1 > \bar{X}_0$

$$P_{\mathrm{D,out}} = \begin{cases} 1-\frac{1}{2}\exp\left\{\dfrac{\bar{X}_0-\bar{X}_1+W_0\ln\left\{2\left(1-P_{\mathrm{F}}\right)/\mathcal{K}_0+\exp\left[\left(X_{\min}-\bar{X}_0\right)/W_0\right]\right\}}{W_{1,\max}-\left(W_{1,\max}-W_{1,\min}\right)P_{\mathrm{out}}}\right\}, & \text{if } X_{\min} \le X_{\mathrm{th}} < \bar{X}_0 \\ 1-\frac{1}{2}\exp\left\{\dfrac{\bar{X}_0-\bar{X}_1-W_0\ln\left\{2\left(\mathcal{K}_0-1+P_{\mathrm{F}}\right)/\mathcal{K}_0-\exp\left[\left(X_{\min}-\bar{X}_0\right)/W_0\right]\right\}}{W_{1,\max}-\left(W_{1,\max}-W_{1,\min}\right)P_{\mathrm{out}}}\right\} & \text{if } \bar{X}_0 \le X_{\mathrm{th}} < \bar{X}_1 \\ \frac{1}{2}\exp\left\{-\dfrac{\bar{X}_0-\bar{X}_1-W_0\ln\left\{2\left(\mathcal{K}_0-1+P_{\mathrm{F}}\right)/\mathcal{K}_0-\exp\left[\left(X_{\min}-\bar{X}_0\right)/W_0\right]\right\}}{W_{1,\min}+\left(W_{1,\max}-W_{1,\min}\right)P_{\mathrm{out}}}\right\} & \text{if } \bar{X}_1 \le X_{\mathrm{th}} \le X_{\max} \end{cases} \tag{7}$$

Proof: The proof is omitted for simplicity.

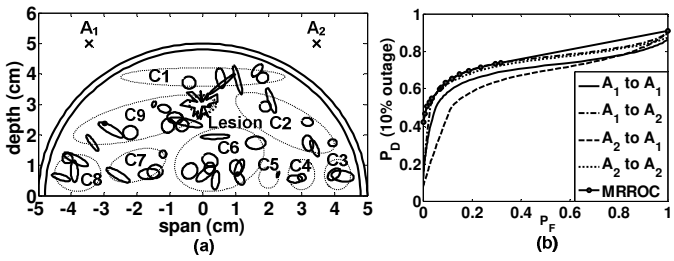

Figure 3: (a) A numerical breast phantom with clustered scatterers [Clusters 1 (C1) - Cluster 9 (C9)]. The dielectric percentage variations for each cluster are as follows: C1: -10%≤μ≤-5%, C2: 0≤μ≤5%, C3: -10%≤μ≤-5%, C4: -10%≤μ≤-5%, C5: -10%≤μ≤-5%, C6: 5%≤μ≤10%, C7: -5%≤μ≤0, C8: -10%≤μ≤-5%, C9: 0≤μ≤5%; (b) ROC curves at 10% outage probability

TABLE I: LESION CLASSIFICATION RESULTS

	P_M	P_F	$(P_M+P_F)/2$
$C_{1,1}(A_1 \to A_1)$	16.7%	26.7%	21.7%
$C_{1,2}(A_1 \to A_2)$	16.7%	10%	13.3%
$C_{2,1}(A_2 \to A_1)$	20%	40%	30%
$C_{2,2}(A_2 \to A_2)$	20%	13.3%	16.7%
Selection combining	16.7%	10%	13.3%

Finally, applying the above results and following Steps (iii) and (iv) give the global decision of the selection combining fusion scheme.

5. CLASSIFICATION RESULTS

The breast geometry that generates test data set for our examples is shown in Fig. 3(a). We consider a simplistic 2×2 MIMO radar architecture. Two antennas A_1 and A_2 are located at ($-2\sqrt{3}$ cm, 5 cm) and ($2\sqrt{3}$ cm, 5 cm), respectively. A_1 transmits an MMHP pulse with $\Omega = 1$, $f_c = 1$ GHz, and $T_p = 50$ ps, while A_2 transmits a pulse with $\Omega = 1$, $f_c = 4$ GHz, and $T_p = 50$ ps. The anomaly is located at (0 cm, 3 cm), which has been estimated *a priori* through a breast cancer detection algorithm [1]. The semi-major and semi-minor axes of the baseline ellipse are 4 mm and 3 mm, respectively. The test data set is created by generating 30 independent target realizations for either OMA or MIS class. The dielectric properties of the clutter items range over ±10%. This numerical phantom also reproduces the effect that the dielectric properties of the healthy tissues exhibit structural differences at different locations [4]. The thickness of the skin layer is 0.2 cm, and the dielectric properties of the nominal and deceased tissues are given in Section 3.

The model parameters of the damping factors for the four diversity paths are obtained based on the results in Section 3. Fig. 3(b) depicts the ROC curves when the outage probability is 10%. It can be seen that no single diversity path produces superior classification performance over the entire range of P_F. Overall, it is expected that the classifiers $C_{1,2}$ ($A_1 \to A_2$) and $C_{2,2}$ ($A_2 \to A_2$) should result in better detection performance as compared to the classifiers $C_{1,1}$ ($A_1 \to A_1$) and $C_{2,1}$ ($A_2 \to A_1$). Fig. 3(b) also shows the MRROC predicted by the convex hull containing other ROC curves, which yield the best performance over the entire range of P_F. The results in Fig. 3(b) clearly demonstrate the advantage of a MIMO radar for lesion classification, which fully explores the information on the phenomenon-of-interest provided by different classifiers to improve the overall performance. The lesion classification results are listed in Table I. We consider the following performance indicators, the probability of miss ($P_M = 1\text{-}P_D$), the probability of false alarm (P_F), and the overall error probability ($(P_M+P_F)/2$). As could be expected, the selection combing fusion achieves the best overall performance. The lesion morphology is classified with 86.7% accuracy averaged over 60 targets. This result is also comparable to the classifier performance reported in [2], where over 70% of the target shapes are correctly classified for 10 dB signal-to-noise ratio.

6. CONCLUSIONS

We have investigated the feasibility of breast tissue discrimination using an UWB MIMO radar imaging system. As a proof-of-concept, we have considered a binary classification of the lesion morphology (OMA versus MIS). The distinct statistical features of the attenuation factors for OMA and MIS targets have been realized through comprehensive simulation studies. Subsequently, the selection combing fusion rule has been proposed to facilitate robust lesion classification. Both the theoretical ROC curves and the simulation results have demonstrated the potential advantage of a MIMO radar architecture for enhanced tissue differentiation.

REFERENCES

[1] X. Li and S. C. Hagness, "A confocal microwave imaging algorithm for breast cancer detection," *IEEE Microw. Wireless Compon. Lett.*, vol. 11, no. 3, pp. 130–132, 2001.

[2] S. K. Davis, B. D. Van Veen, S. C. Hagness, and F. Kelcz, "Breast tumour characterization based on ultrawideband microwave backscatter," *IEEE Trans. Biomed. Eng.*, vol. 55, pp. 237–246, Jan. 2008.

[3] Y. Chen, E. Gunawan, K. S. Low, S.-C. Wang, C. B. Soh, and T. C. Putti, "Effect of lesion morphology on microwave signature in 2-D ultra-wideband breast imaging," *IEEE Trans. Biomed. Eng.*, vol. 55, no. 8, pp. 2011–2021, 2008.

[4] M. Lazebnik, D. Popovic, L. McCartney, and *et al.*, "A large-scale study of the ultrawideband microwave dielectric properties of normal, benign and malignant breast tissues obtained from cancer surgeries," *Physics in Medicine and Biology*, vol. 52, pp. 6093–6115, 2007.

[5] R. M. Rangayyan, N. M. El-Faramawy, J. E. Leo Desautels, and O. A. Alim, "Measures of acutance and shape for classification of breast tumors," *IEEE Trans. Med. Imag.*, vol. 16, no. 6, pp. 799–810, 1997.

[6] J. Li and P. Stoica, "MIMO radar with collocated antennas," *IEEE Signal Processing Mag.*, vol. 24, no. 5, pp. 106–114, 2007.

[7] M. Ghavami, L. B. Michael, S. Haruyama, and R. Kohno, "A novel UWB pulse shape modulation system," *Springer Wireless Personal Communications*, vol. 23, pp. 105–120, 2002.

[8] T.M. Cover and J. A. Thomas, *Elements of Information Theory*, John Wiley and Sons, Inc., 1991.

[9] V. V. Veeravalli, T. Bas¸ar, and H. V. Poor, "Minimax robust decentralized detection," *IEEE Trans. Inform. Theory*, vol. 40, no. 1, pp. 35–40, 1994.

[10] M. J. J. Scott, M. Niranjan, and R. W. Prager, "Realisable classifiers: Improving operating performance on variable cost problems," *Proc. Ninth British Machine Vision Conference*, vol. 1, pp. 304–315, 1994.